ELSEVIER

# Numerical simulation of turbulence suppression: Comparisons of the performance of four $k$–$\varepsilon$ turbulence models

**J. C. S. Lai and C. Y. Yang**
School of Aerospace and Mechanical Engineering, University College, The University of New South Wales, Australian Defence Force Academy, Canberra, Australia

The standard $k$–$\varepsilon$ model and three low-Reynolds number $k$–$\varepsilon$ models were used to simulate pipe flow with a ring device installed in the near-wall region. Both developing and fully developed turbulent pipe flows have been investigated. Turbulence suppression for fully developed pipe flows revealed by hot-wire measurements has been predicted with all three low-Reynolds number models, and turbulence enhancement has been predicted by the standard $k$–$\varepsilon$ model. All three low-Reynolds number models have predicted similar distributions of velocities, turbulence kinetic energy, and dissipation rate. For developing pipe flows, the region of turbulence suppression predicted by the three low-Reynolds number models is much more extensive (up to 30 pipe diameters downstream of the device) than for full developed flow; whereas the standard $k$–$\varepsilon$ model has only predicted turbulence enhancement. © 1997 by Elsevier Science Inc.

**Keywords:** turbulence suppression; turbulence, models; pipe flows; large-eddy break-up

## Introduction

Since the identification of coherent structures in a variety of fluid flows, considerable efforts have been devoted to controlling these structures using either active or passive means for practical applications. Large-eddy break-up (LEBU) devices have been studied for drag reduction purposes (Savill and Mumford 1988). While there has been considerable debate in the past as to whether LEBU device produces net drag reduction (Prabhu et al. 1987; Sahlin et al. 1987; Sahlin et al. 1988), there is now general consensus that a LEBU device does induce reduction in the skin friction drag in the flow being manipulated, although the drag introduced by such a device may more than offset such reduction (Squire and Savill 1996).

Numerous studies have been conducted for external boundary-layer flows (for obvious applications such as aircraft, ships, etc.) to determine the optimum dimensions, locations, amount of skin friction reduction, and the mechanism by which such reduction is achieved. For a review of these studies, see, for example, Savill and Mumford (1988), Wark et al. (1990). Coustols and Savill (1992), and Squire and Savill (1996). By contrast, relatively little attention has been paid to internal flows. Experiments on plate-manipulated channel flows and pipe flows include those reported by Prabhu et al. (1987), Pollard et al. (1989, 1990), Mah et al. (1992), Hollis et al. (1992) and Khoo et al. (1993). Because the purpose of a LEBU device is to break up the large eddies, it is usually located in the outer boundary layer. However, Hollis et al. (1992) argues that for internal flows, the device should be installed in the near-wall region where dominant shear-stress production occurs. They conducted experiments in full developed pipe flow with a ring device installed at $y^+ = 112$, which was at least an order of magnitude closer to the wall than any other studies available in the literature. The Reynolds number was 225,000 (based on pipe diameter and average velocity), and measurements were made at at least 55 pipe diameters, where the flow was already fully developed. The difference between the axial turbulence intensity with and without the device installed obtained by Hollis et al. is normalized by the axial turbulence intensity without the device and is plotted as contours in Figure 1. It can be seen that immediately downstream of the device, the axial turbulence intensity with the device installed is higher than that without the device and the increase in turbulence is diffusing away from the wall. However, for $x^+ > 500$, the axial turbulence intensity with the device installed is significantly lower than that without the device; in particular, in the region bounded by $500 < x^+ < 2000$ and $20 < y^+ < 100$, the decrease is over 40%. Furthermore, although experimental results were not obtained downstream of $x^+ = 5500$, it appears from Figure 1 that the region of axial turbulence intensity suppression extends beyond $x^+ = 5500$. The objective of this investigation was, therefore, to

Address reprint requests to Dr. J. C. S. Lai, Australian Defence Force Academy, School of Aerospace and Mechanical Engineering, Canberra ACT 2600, Australia.

Received 3 July 1996; accepted 23 January 1997

Int. J. Heat and Fluid Flow 18: 575–584, 1997

655 Avenue of the Americas, New York, NY 10010

0142-727X/97/$17.00
PII S0142-727X(97)00003-9

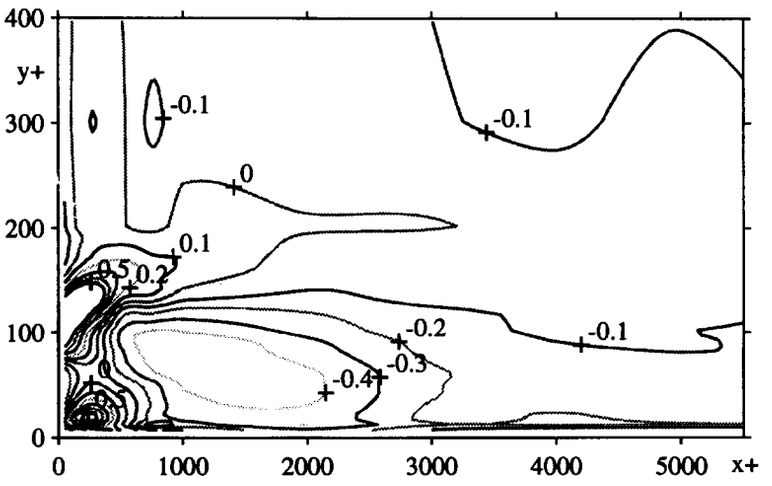


*Figure 1* Contours of nondimensional axial turbulence intensity differences between fully developed turbulent pipe flow with and without a ring device.

study numerically the phenomenon of turbulence suppression in fully developed and developing turbulent pipe flow attributable to a ring device installed in the near-wall region.

Some approaches that can be used for studying this phenomenon of turbulence suppression include direct numerical simulation (DNS), large-eddy simulations (LES), and solving the Reynolds-averaged Navier–Stokes equations using statistical turbulence models. Although DNS offer insight into the mechanism of drag reduction (Kim et al. 1990), it is restricted to calculations of flows with low Reynolds numbers, generally less than 10,000. By using LES data for manipulated channel flows, Savill et al. (1993) showed that pattern recognition analysis of structures can help understanding the effects of introducing manipulators on flow structures. There is, therefore, potential in using LES data to provide further understanding of the mechanism of skin friction reduction achieved by manipulators and to optimise control of these flow structures. Nevertheless, LES data cannot provide information regarding small-scale interactions. Pollard et al. (1989, 1990) conducted some parametric studies of turbulent pipe flows manipulated by ring devices using a low-Reynolds number $k$–$\varepsilon$ model proposed by Lam and Bremhorst (1981). In this paper, we chose to examine how four different $k$–$\varepsilon$ models perform in simulating the phenomenon of turbulence suppression in fully-developed pipe flows observed by Hollis et al. (1992).

Of the models used to predict turbulent flows, the most popular is the two-equation $k$–$\varepsilon$ model. The standard $k$–$\varepsilon$ model developed by Launder and Spalding (1974) for high-Reynolds number flows employs wall functions. Because many important technological applications require the use of turbulence models directly extended to a solid boundary, Lam and Bremhorst (1981) and several other researchers have extended the original $k$–$\varepsilon$ model to the low-Reynolds number (Re) form, which allows calculations right to the wall. In a systematic study, Patel et al. (1985) found that the low-Reynolds number $k$–$\varepsilon$ models of Lam and Bremhorst, Launder and Sharma (1974), and Chien (1982) and the model of Wilcox and Rubesin (1980) perform considerably better than others. These low-Reynolds number $k$–$\varepsilon$ models are essentially similar to that of Lam and Bremhorst, except for the specific choice of the damping functions $f_\mu$, $f_1$, and $f_2$. Owing to a lack of reliable experimental data, these near-wall modifications have largely been based on dimensional reasoning, intuition, and indirect testing. As pointed out by Rodi and

## Notation

| | |
|---|---|
| $c_1, c_2, c_\mu$ | Turbulence model constants |
| $C_f$ | friction coefficient $= \tau w / \frac{1}{2}\rho U_b^2$ |
| $D$ | diameter of pipe |
| $E$ | function defined in Table 1 |
| $f_1, f_2, f_\mu$ | turbulence model functions |
| $G_k$ | function defined in Equation 5 |
| $k$ | turbulence kinetic energy |
| $K$ | total turbulence kinetic energy |
| $l^+$ | nondimensional length of the ring device |
| $p$ | pressure |
| $r$ | radial coordinate |
| $R$ | radius of pipe |
| $R_k$ | turbulence Reynolds number $= \rho\sqrt{k}y/m$ |
| $R_t$ | turbulence Reynolds number $= \rho k^2/\mu\varepsilon$ |
| $R_p$ | $= G_k/k\sqrt{c_\mu \epsilon/\nu}$ |
| $u$ | axial mean velocity |
| $U_b$ | average inlet velocity |
| $t^+$ | nondimensional thickness of the ring device |
| $u^+$ | nondimensional axial mean velocity |
| $u_\tau$ | friction velocity |
| $v$ | radial mean velocity |
| $x$ | axial coordinate |
| $y$ | normal distance from the wall |
| $y^+$ | nondimensional distance from the wall $(yu_\tau/\nu)$ |

*Greek*

| | |
|---|---|
| $\varepsilon$ | turbulence dissipation rate |
| $\mu$ | dynamic viscosity |
| $\kappa$ | von Karman's constant |
| $\mu_t$ | turbulence eddy-viscosity |
| $\mu_{\text{eff}}$ | effective viscosity |
| $\nu$ | kinematic viscosity |
| $\rho$ | density |
| $\sigma_k, \sigma_\varepsilon$ | turbulence Prandtl–Schmidt numbers |
| $\tau_w$ | wall shear stress |

*Subscripts*

| | |
|---|---|
| d | with device |
| nd | without device |

Mansour (1993), even the more established models fail to reproduce the near-wall flow characteristics in detail. Thus, Rodi and Mansour deduced new forms of $k$–$\varepsilon$ model based on DNS data. In an effort to overcome some of the deficiencies of $k$–$\varepsilon$ models (such as arbitrary definition of near-wall pseudodissipation rate, the inability to handle separation flows, and the inability to handle well flows that involve both high-Reyolds number turbulence and near-wall turbulence), a new time-scale-based $k$–$\varepsilon$ model for near-wall turbulence was proposed by Yang and Shih (1993).

In this study, therefore, the standard $k$–$\varepsilon$ model (LS) developed by Launder and Spalding (1974), the Lam and Bremhorst model (1981) (LB), the Rodi and Mansour model (1993)) (RM), and the Yang and Shih (1993) new time-scale-based $k$–$\varepsilon$ model (YS) were used to investigate developing and fully developed turbulent pipe flows at Re = 240,000, with a ring device located at $y^+ = 112$. It should be emphasised that the location of the ring device in this study was at least one order of magnitude closer to the wall than those locations studied by Pollard et al. (1989, 1990). Comparisons of mean velocity distributions in fully developed pipe flows are made between predictions and the measurements of Hollis et al. (1992). The performance of each model in simulating this type of flow is discussed. In particular, the ability of these models to predict the phenomenon of turbulence suppression is examined.

## Governing equations

Consider a ring device installed in a pipe, as shown in Figure 2. In cylindrical coordinates, the Reynolds time-averaged momentum and continuity equations are given by Equations 1–3 (see, for example, Pun and Spalding (1976)). The effective viscosity

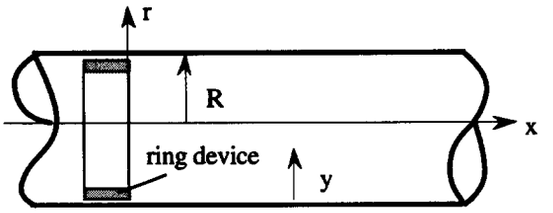


*Figure 2* Schematic diagram of the flow geometry

$\mu_{\text{eff}}$ is given by $(\mu + \mu_t)$. For the four turbulence models used here, the turbulent viscosity $\mu_t$ is determined from $\mu_t = c_\mu f_\mu \rho k^2/\varepsilon$ with $k$ and $\varepsilon$ to be computed from the modelled transport Equations 4 and 5 for $k$ and $\varepsilon$, respectively. While the constants $c_1 = 1.45$, $c_2 = 1.90$, and $c_\mu = 0.09$ are the same for the four turbulence models considered here, the other constants and functions for each model are summarised in Table 1.

*x-direction*:

$$\frac{\partial}{\partial x}(\rho uu) + \frac{1}{r}\frac{\partial}{\partial r}(\rho rvu) - \frac{\partial}{\partial x}\left(\mu_{\text{eff}}\frac{\partial u}{\partial x}\right) - \frac{1}{r}\frac{\partial}{\partial r}\left(r\mu_{\text{eff}}\frac{\partial u}{\partial r}\right) = S_u \tag{1}$$

*r-direction*:

$$\frac{\partial}{\partial x}(\rho uv) + \frac{1}{r}\frac{\partial}{\partial r}(\rho rvv) - \frac{\partial}{\partial x}\left(\mu_{\text{eff}}\frac{\partial v}{\partial x}\right) - \frac{1}{r}\frac{\partial}{\partial r}\left(r\mu_{\text{eff}}\frac{\partial v}{\partial r}\right) = S_v \tag{2}$$

**Table 1** Turbulence model functions and constants

| Constants/functions | Model | | | |
|---|---|---|---|---|
| | LS | LB | RM | YS |
| $\varepsilon_w$ | Wall function | $\nu\frac{\partial^2 k}{\partial y^2}$ | $2\nu\left(\frac{\partial\sqrt{k}}{\partial y}\right)^2$ | $2\nu\left(\frac{\partial\sqrt{k}}{\partial y}\right)^2$ |
| $\sigma_k$ | 1.0 | 1.0 | 1.3 | 1.0 |
| $\sigma_\varepsilon$ | 1.3 | 1.3 | 1.3 | 1.3 |
| $T$ | $\frac{k}{\varepsilon}$ | $\frac{k}{\varepsilon}$ | $\frac{k}{\varepsilon}$ | $\frac{k}{\varepsilon}+c_k\left(\frac{\nu}{\varepsilon}\right)^{1/2}$ |
| $E$ | 0 | 0 | $1.2\nu\nu_t\left(\frac{\partial^2 u}{\partial y^2}\right)^2$ $-0.0075\nu\frac{k}{\varepsilon}\frac{\partial k}{\partial y}\frac{\partial u}{\partial y}\frac{\partial^2 u}{\partial y^2}$ | $\nu\nu_t\left\{\left(\frac{\partial^2 u}{\partial x^2}\right)^2+\left(\frac{\partial^2 u}{\partial y^2}\right)^2+\left(\frac{\partial^2 v}{\partial x^2}\right)^2+\left(\frac{\partial^2 v}{\partial y^2}\right)^2+2\left[\left(\frac{\partial^2 u}{\partial x\partial y}\right)^2+\left(\frac{\partial^2 v}{\partial x\partial y}\right)^2\right]\right\}$ |
| $f_\mu$ | 1.0 | $[1.-\exp(-0.0165R_y)]^2\cdot\left(1+\frac{20.5}{R_t}\right)$ | $y^+<100$: $[1-\exp(2\cdot10^{-4}y^+ -6\cdot10^{-4}y^{+2} +2.5\cdot10^{-7}y^{+3})]$ $y^+\geq 100$:1.0 | $[1.-\exp(-1.5\cdot10^{-4}R_y -5.0\cdot10^{-7}R_y^3 -1.0\cdot10^{-10}R_y^5)]^{1/2}$ |
| $f_1$ | 1.0 | $1+\left(\frac{0.05}{f_\mu}\right)^3$ | 1.0 | 1.0 |
| $f_2$ | 1.0 | $1-\exp(-R_t^2)$ | $[1-0.22\exp(0.3357R_t^{1/2})]\cdot[1-\exp(-0.095R_y)] +\exp(1.8R_\rho^3)-1$ | 1.0 |

*continuity*:

$$\frac{\partial(\rho u)}{\partial x}+\frac{1}{r}\frac{\partial(\rho r v)}{\partial r}=0 \tag{3}$$

where

$$S_u=\frac{\partial}{\partial x}\left(\mu_{\text{eff}}\frac{\partial u}{\partial x}\right)+\frac{1}{r}\frac{\partial}{\partial r}\left(r\mu_{\text{eff}}\frac{\partial v}{\partial x}\right)-\frac{\partial p}{\partial x}$$

$$S_v=\frac{\partial}{\partial x}\left(\mu_{\text{eff}}\frac{\partial u}{\partial r}\right)+\frac{1}{r}\frac{\partial}{\partial r}\left(r\mu_{\text{eff}}\frac{\partial v}{\partial r}\right)-2\mu_{\text{eff}}\frac{v}{r^2}-\frac{\partial p}{\partial r}$$

$k$:

$$\frac{\partial}{\partial x}(\rho u k)+\frac{1}{r}\frac{\partial}{\partial r}(\rho r v k)-\frac{\partial}{\partial x}\left[\left(\mu+\frac{\mu_t}{\sigma_k}\right)\frac{\partial k}{\partial x}\right]$$

$$-\frac{1}{r}\frac{\partial}{\partial r}\left[r\left(\mu+\frac{\mu_t}{\sigma_k}\right)\frac{\partial k}{\partial r}\right]=G_k-\rho\varepsilon \tag{4}$$

$\varepsilon$:

$$\frac{\partial}{\partial x}(\rho u\varepsilon)+\frac{1}{r}\frac{\partial}{\partial r}(\rho r v\varepsilon)-\frac{\partial}{\partial x}\left[\left(\mu+\frac{\mu_t}{\sigma_\varepsilon}\right)\frac{\partial \varepsilon}{\partial x}\right]$$

$$-\frac{1}{r}\frac{\partial}{\partial r}\left[r\left(\mu+\frac{\mu_t}{\sigma_\varepsilon}\right)\frac{\partial \varepsilon}{\partial r}\right]$$

$$=(c_1 f_1 G_k-c_2 f_2\rho\varepsilon)/T+E \tag{5}$$

where

$$G_k=\mu_{\text{eff}}\left\{2\left[\left(\frac{\partial u}{\partial x}\right)^2+\left(\frac{\partial v}{\partial r}\right)^2+\left(\frac{v}{r}\right)^2\right]+\left(\frac{\partial u}{\partial r}+\frac{\partial v}{\partial x}\right)^2\right\}$$

## Boundary conditions

Because of the elliptic nature of the conservation equations, boundary conditions must be specified at all boundaries of the domain considered.

### *Inlet*

The inlet conditions are defined by prescribed distributions of velocity, turbulence kinetic energy, and dissipation rate. For developing flows, the inlet conditions are uniform velocity profile with the inlet kinetic energy and dissipation rate being given by (Pun and Spalding 1976):

$$k=0.005U_b^2 \qquad \varepsilon=c_\mu k^{3/2}/(0.03R)$$

For fully developed flows, the inlet velocity, kinetic energy, and dissipation rate distributions used are those calculated for fully developed pipe flows.

### *Exit*

At the outlet boundary, the flow is assumed to be fully developed and $v$ is set to zero; i.e.,

$$\frac{\partial u}{\partial x}=\frac{\partial k}{\partial x}=\frac{\partial \varepsilon}{\partial x}=0 \qquad v=0$$

### *Axis of symmetry*

Zero gradient boundary conditions are applied at the axis of symmetry where the transverse velocity component $v$ must also vanish.

$$\frac{\partial u}{\partial r}=\frac{\partial k}{\partial r}=\frac{\partial \varepsilon}{\partial r}=0 \qquad v=0$$

### *Wall*

In the near-wall region, the standard $k$–$\varepsilon$ model (LS) employs a wall function. Based on the log-law of the wall; and assuming equilibrium conditions in the turbulent boundary layer, the following expression can be derived (Pun and Spalding (1976)):

$$y^+=\frac{c_\mu^{0.25}\rho\sqrt{k}\,y}{\mu} \qquad y^+>11.5$$

$$\tau_w=\frac{\kappa c_\mu^{0.25}\rho u_P\sqrt{k_P}}{\ln(Ey^+)} \qquad y^+>11.5$$

$$\tau_w=\mu u_p/\delta \qquad y^+\le 11.5$$

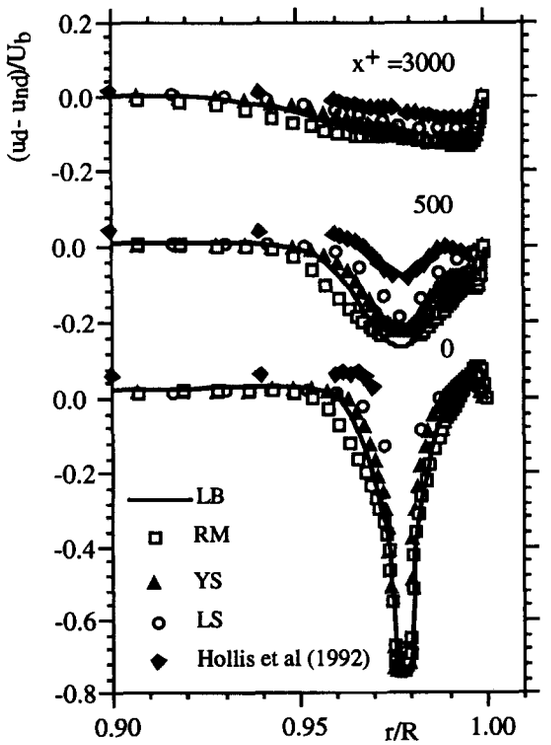


*Figure 3* Variation of nondimensional velocity differences with $r/R$

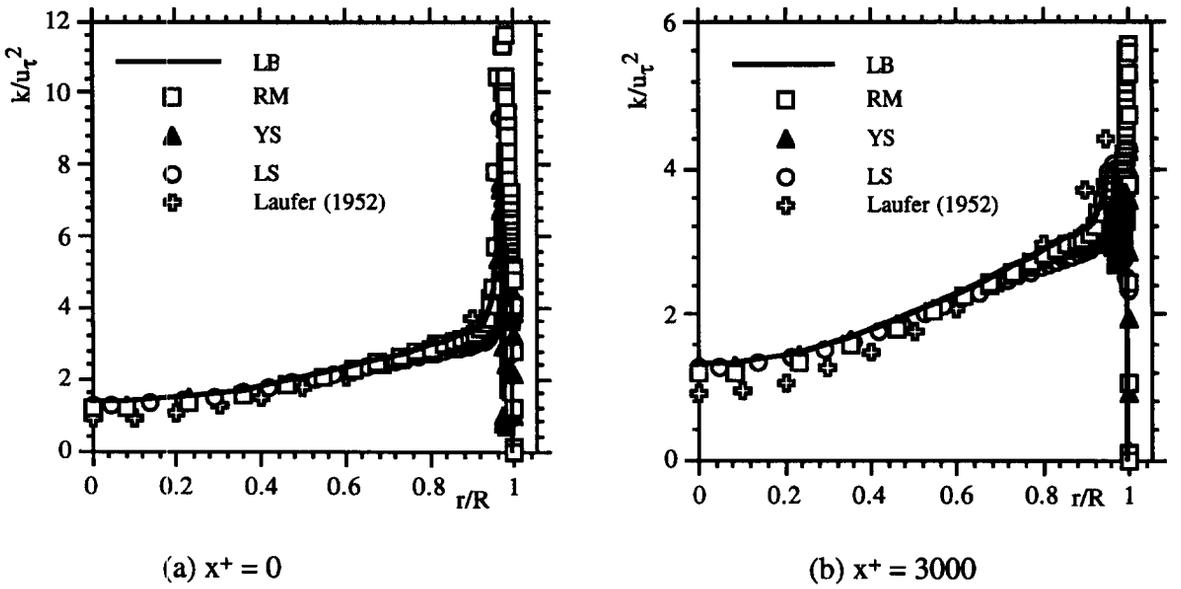


*Figure 4* Distributions of turbulence kinetic energy for fully developed flow with a ring device; (a) $x^+=0$; (b) $x^+=3000$

where $\kappa = 0.4$, $E = 9.0$ for smooth walls; $k_P$ and $u_P$ are turbulence kinetic energy and velocity at the grid points directly adjacent to the wall, respectively. For the LB, RM, and YS models, the physical boundary conditions for $k$ and $\varepsilon$ are directly implemented; i.e., $k_{wall} = 0$, with $\varepsilon_{wall}$ being listed in Table 1.

## Results

The conservation and modelled transport equations were discretised and solved using the SIMPLE (Semi-implicit method pressure-linked equations) algorithm (Patankar 1980). The computational domain covers $0 \leq r/R \leq 0.5$ and $0 \leq x/D \leq 60$. Nonuniform grids were used for all four models, with $99 \times 38$ grid points for the LS model and $143 \times 87$ grid points for the LB, RM, and YS models. The computer codes were first validated by computing full developed turbulent pipe flows without the installation of a ring device. Grid dependency was investigated by calculating turbulent fully developed pipe flow using various grid distributions for the LS model. Results documented by Yang and Lai (1993) indicate that the maximum differences in the axial velocity distributions and skin friction coefficient for $34 \times 34$ and $66 \times 66$ grids are less than 1%, thus justifying the use of $99 \times 38$ grid for the LS model. Yang and Lai showed that the calculations for fully developed turbulent pipe flow using a $120 \times 67$ grid for the LB model are in good agreement with the experimental data of Richman and Azad (1973) and Nikuradse (1933). Furthermore, Pollard et al. (1989) used a grid of $150 \times 67$ to study plate-manipulated turbulent pipe flow using the LB model. Thus, a grid of $143 \times 87$ is considered adequate for the calculations using the LB, RM, and YS models. All the calculations reported here were performed on SUN SPARC 1000 workstation for pipe flow

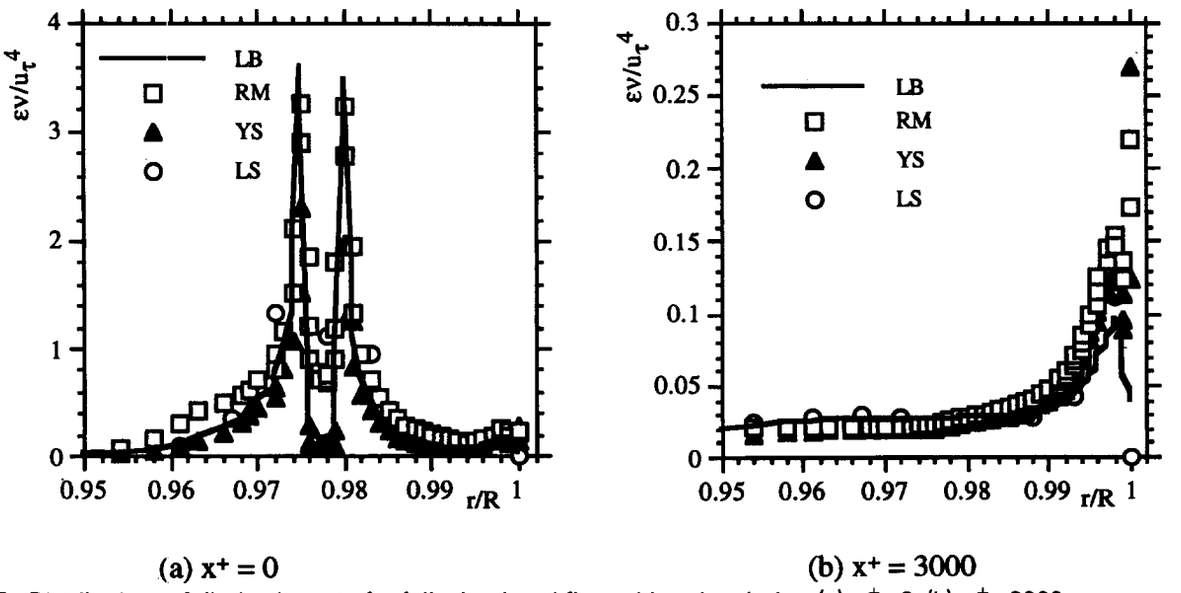


*Figure 5* Distributions of dissipation rate for fully developed flow with a ring device; (a) $x^+=0$; (b) $x^+=3000$

Reynolds number Re = 240,000, friction velocity $u_\tau = 0.61$ m/s, with a ring device of length 10 mm ($l^+ = 400$) and thickness 0.635 mm ($t^+ = 25$) installed at $y^+ = 112$.

### *Fully developed flow*

**Velocity distributions.** Figure 3 shows the radial distribution of non dimensional mean velocity differences, defined as $(u_d - u_{nd})/U_b$, at various axial distances downstream of the device. Here $u_d$ and $u_{nd}$ refer to the axial mean velocity in a flow with and without a ring device, respectively. The effect of the ring device on the velocity distributions can be clearly seen from Figure 1, particularly at the trailing edge of the ring device ($x^+ = 0$), where the velocity defect in the wake is prominent. The velocity distributions start recovering as the flow proceeds downstream. The results of all four models are close to each other. Although the numerical results agree qualitatively with the trend of the experimental data of Hollis et al. (1992), there are significant differences between the numerical and experimental results close to the device. However, by $x^+ = 3000$, the agreement between numerical predictions and experimental data has improved significantly.

**Turbulence kinetic energy distributions.** Figures 4(a) and (b) display the distributions of nondimensional turbulence kinetic

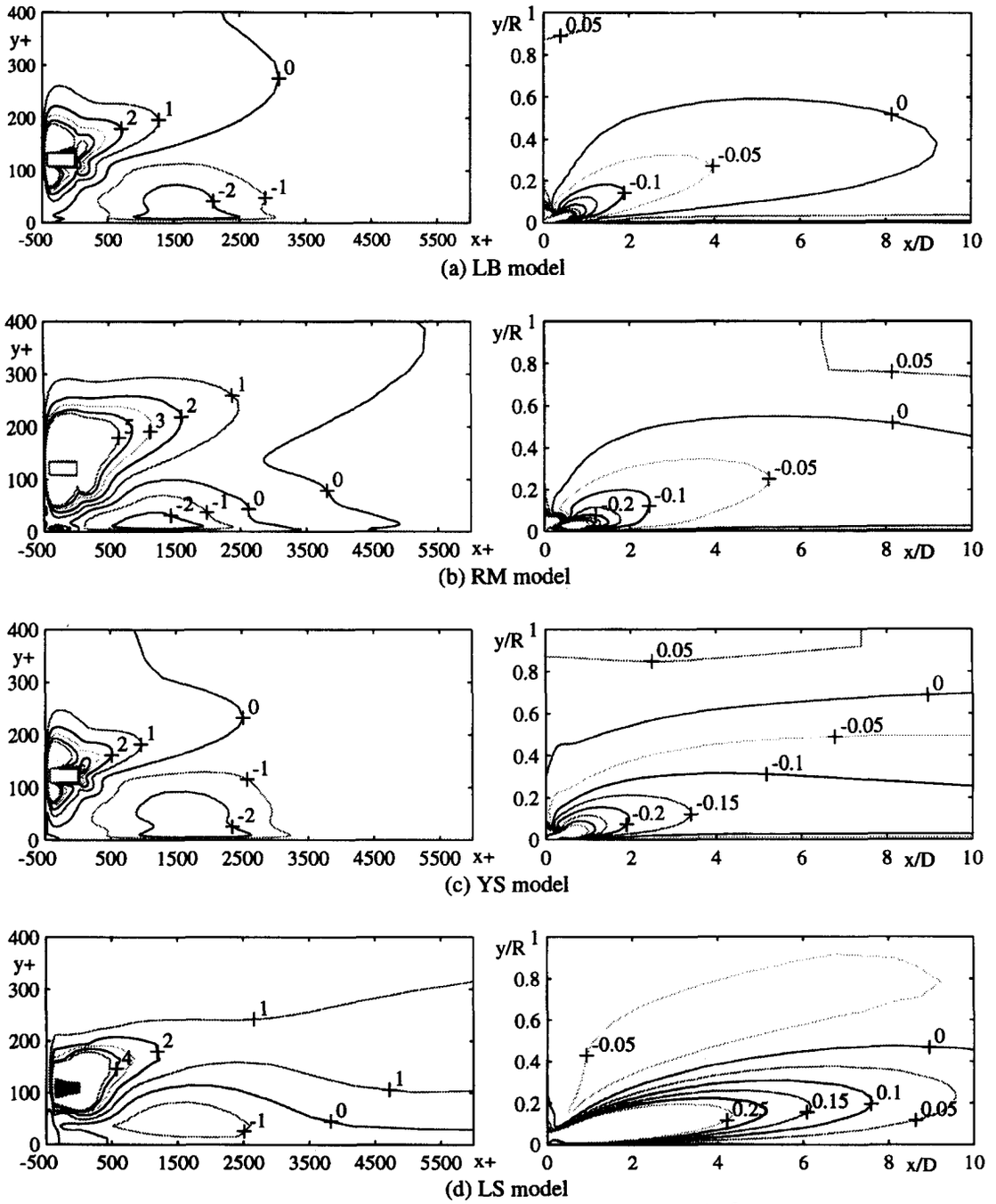


*Figure 6* Contours of nondimensional turbulence kinetic energy difference $(k_d - k_{nd})/u_\tau^2$ for fully developed flow with a ring device

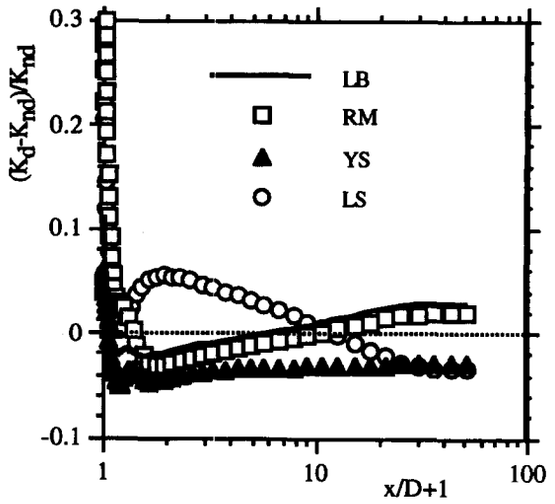


*Figure 7* Variation of turbulence suppression with downstream distance for fully developed flow

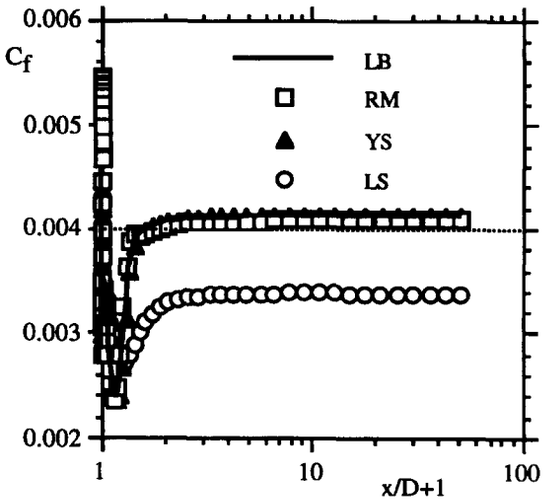


*Figure 8* Variation of skin friction with downstream distance for fully developed flow

energy at $x^+ = 0$ and 3000, respectively. Experimental data of Laufer (1954) for fully developed pipe flow are also plotted in Figures 4(a) and (b) for comparison. It can be seen from Figure 4(a) that the turbulence kinetic energy close to the wall (that is, near the device) is substantially higher than that for full developed pipe flow without a device. However, by $x^+ = 3000$ (Figure 4b), the turbulence kinetic energy near the wall as predicted by the LB, YS, and LS models has decayed so much that it is below the data of Laufer (1954) for fully developed flow. Although there are virtually no differences between the predictions of turbulence kinetic energy for all the four models at $x^+ = 3000$ and for $r/R < 0.9$, the results of the RM model near the wall ($r/R > 0.9$) are higher than those of the other three models.

**Distribution of dissipation rate.** The radial distributions of nondimensional dissipation rate at $x^+ = 0$ and 3000 are shown in Figures 5a and b, respectively. Near the device, at $x^+ = 0$ and $r/R \approx 0.98$, both the YS and LS models predict a much lower dissipation rate, as compared with the LB and RM models. By $x^+ = 3000$, the differences between all four models are quite small except near the wall ($r/R > 0.99$), where the RM and YS models yield a dissipation rate much more compatible with the physics than that obtained with the LB model.

**Turbulence suppression and skin friction reduction.** As shown in Figure 4b, suppression of turbulence kinetic energy near the wall is predicted by all four models. To examine the extent of turbulence suppression, the difference between the turbulence kinetic energy for the flow with and without a ring device ($k_d - k_{nd}$) is nondimensionalised by $u_\tau^2$, and plotted as contours in Figure 6 for all the four models. Note that for each model, contours are plotted for both the near-wall region and for the whole flow field up to 10 pipe diameters downstream of the device.

For the near-wall region, Figure 6 shows that all four models predict an increase in turbulence kinetic energy immediately downstream of the device, and this increase is diffusing away from the wall. Furthermore, all four models predict a region of reduction in turbulence kinetic energy between the device and the wall, which seems to extend up to and beyond $x^+ = 6000$. However, the extent of this region of turbulence suppression

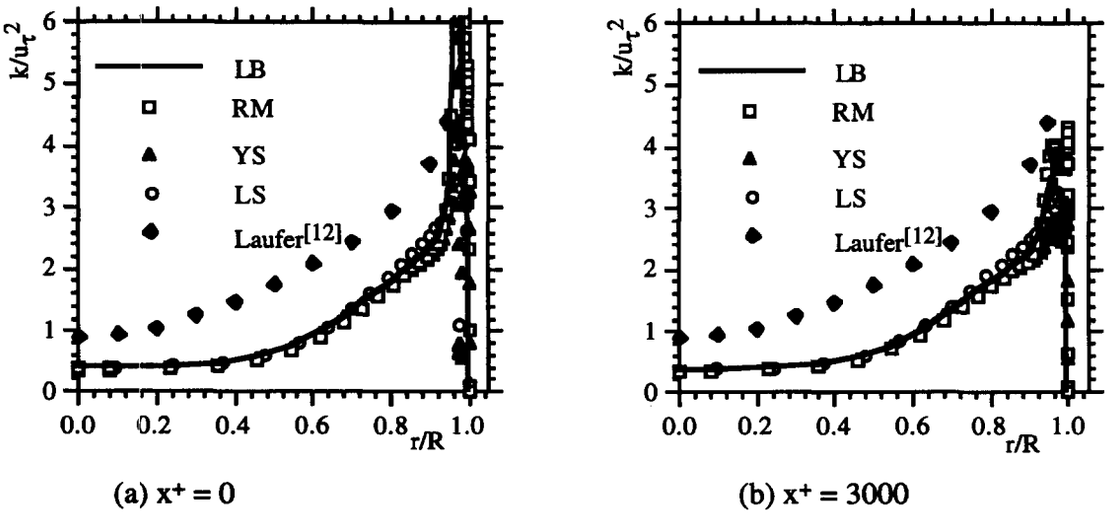


*Figure 9* Distribution of turbulence kinetic energy for developing pipe flow; (a) $x^+ = 0$; (b) $x^+ = 3000$

differs between the various models. Although, strictly speaking, it is incorrect to compare Figure 1 (which shows the nondimensional axial turbulence intensity difference determined by experiments) directly with Figure 6 (which shows the nondimensional turbulence kinetic energy difference predicted numerically), there are remarkable similarities between the numerical and experimental results. While the experiments only measured one component of the turbulence intensities, the numerical results in Figure 6 suggest that turbulence kinetic energy is, indeed, suppressed by a ring device installed near the wall.

Farther downstream from the device, Figure 6 shows that turbulence suppression and enhancement, indeed, occur in different regions of the flow. For LB, RM, and YS models, turbulence suppression occurs primarily in the region $0 < y/R < 0.55$ and up to and beyond $x/D = 10$, while turbulence enhancement occurs in the region $0.55 < y/r < 1$. On the other hand, the results of the LS model in Figure 6d show the opposite trend, where turbulence enhancement occurs between the wall and approximately $0.4R$ and turbulence suppression takes place further away from the wall and closer to the centre line of the pipe.

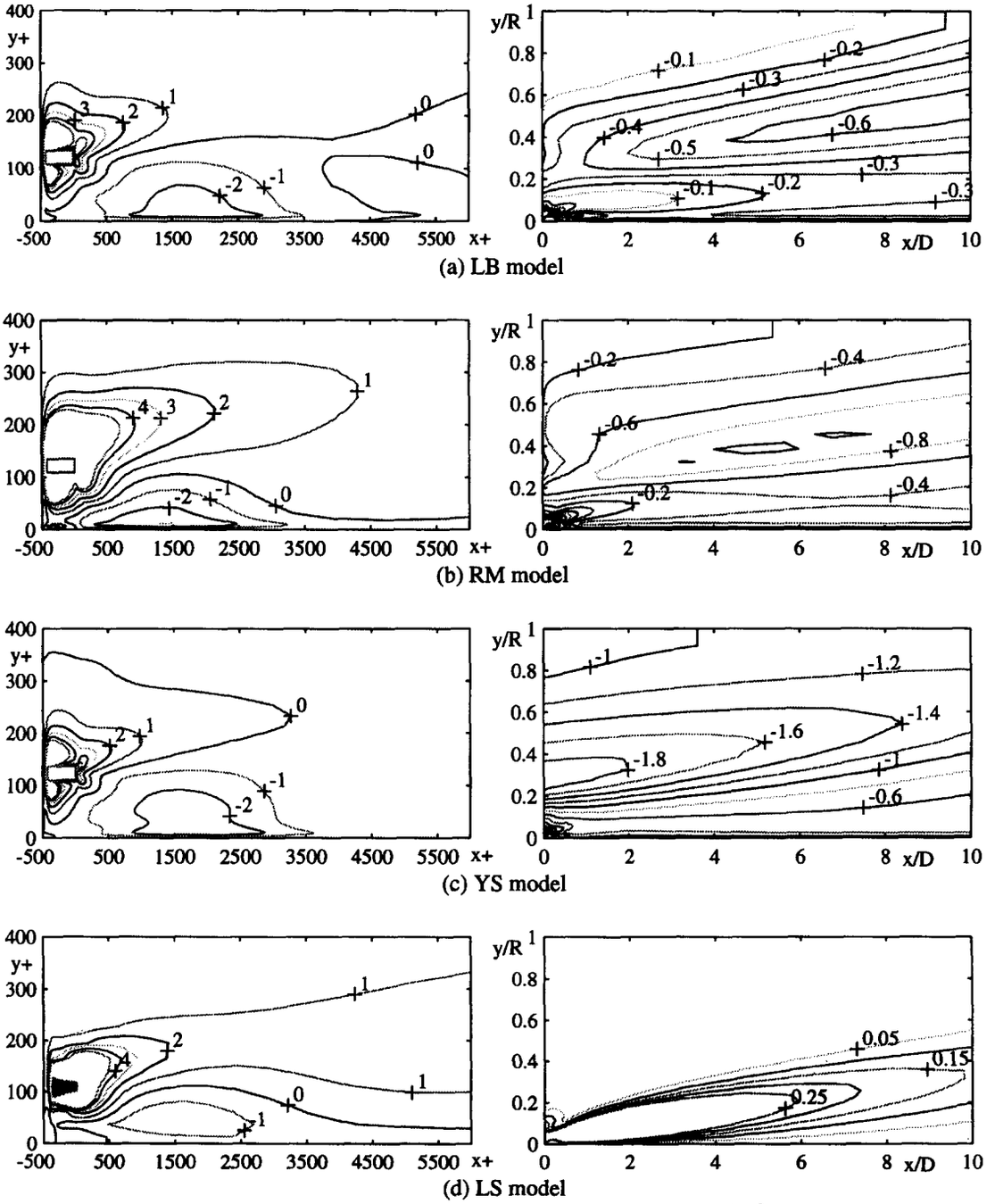


*Figure 10* Contours of nondimensional turbulence kinetic energy difference $(k_d - k_{nd})/u_\tau^2$ for developing flow with a ring device

To quantify the degree of turbulence suppression (or enhancement), the turbulence kinetic energy ($K$) at each streamwise distance is defined as

$$\int_0^R 2\pi r k\, dr$$

Figure 7 shows the variation of the nondimensional turbulence kinetic energy difference, defined as $(K_d - K_{nd})/K_{nd}$, with streamwise distances. It can be seen that both LB and RM models predict turbulence suppression up to $x/D = 9$, while the YS model predicts turbulence suppression up to $x/D = 50$. However, the maximum turbulence kinetic energy suppression is about 5%. On the other hand, Figure 7 shows that the LS model predicts turbulence enhancement up to $x/D = 9$, and the maximum turbulence enhancement is over 5%.

With the suppression of turbulence kinetic energy, it is expected that there should be some skin friction reduction. As shown in Figure 8, the skin friction coefficient $C_f$ calculated by the LB, RM, and LS models for fully developed flow manipulated with a ring device increases to above that for the fully developed pipe flow near the device. However, there is a reduction in $C_f$ immediately downstream of the device, but by $x/D \approx 1$, $C_f$ has recovered to its value for fully developed flow without a device. Skin friction is reduced by as much as 40% at a few device lengths downstream of the device. The results of LB, RM, and YS models agree with each other very well. Although Figure 7 shows turbulence enhancement for the LS model, skin friction reduction is also predicted by the LS model, as shown in Figure 8. It should be noted that the LS model yields lower $C_f$ than the other three models.

### *Developing pipe flow*

**Turbulence kinetic energy distributions.** The radial distributions of nondimensional turbulence kinetic energy for $x^+ = 0$ and $x^+ = 3000$ in developing pipe flow installed with a ring device are shown in Figures 9a and b, respectively. As expected, the turbulence kinetic energy at $x^+ = 0$ is very high and has exceeded the values near the wall measured by Laufer (1954) for fully developed pipe flow. By $x^+ = 3000$, however, the turbulence kinetic energy has been reduced significantly, particularly near the wall.

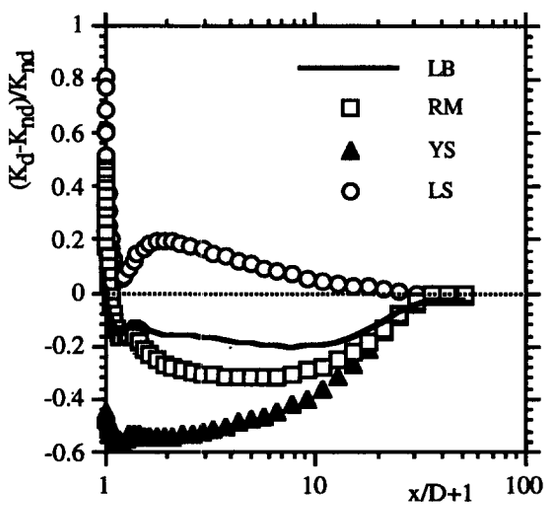


*Figure 11* Variation of turbulence suppression with downstream distances for developing pipe flow

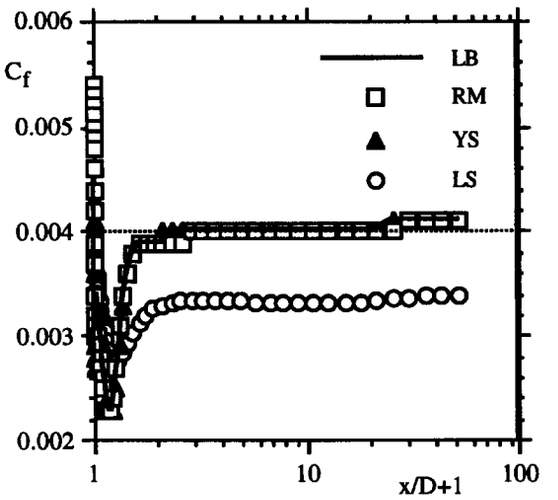


*Figure 12* Variation of skin friction with downstream distances for developing pipe flow

**Turbulence suppression and skin friction reduction.** Contours of nondimensional turbulence kinetic energy difference, defined as $(k_d - k_{nd})/u_\tau^2$, are shown in Figure 10 for all four models in both the near-wall region and the whole flow region up to $x/D = 10$. It can be seen that the distribution of turbulence suppression and enhancement in the near-wall region is very similar to that for fully developed flow shown in Figure 6. However, as the flow is developing, it is expected that the development downstream could be be quite different from that of the fully developed flow shown in Figure 6. Indeed, Figure 10 indicates that for LB, RM, and YS models, turbulence suppression is predicted up to and beyond $x/D = 10$ for the whole pipe flow region instead of being confined to a region between the wall and $y/R \approx 0.55$ (as in full developed flow). On the other hand, the LS model actually predicts turbulence enhancement for the whole flow field up to $x/D = 10$, except very near the wall and close to the device.

The variation of the suppression of turbulence kinetic energy for developing pipe flow, expressed as $(K_d - K_{nd})/K_{nd}$, with streamwise distance is shown in Figure 11. All three low-Reynolds number models predict turbulence suppression up to $x/D \approx 30$ with maximum suppression of almost 60% predicted by the YS model. On the other hand, the standard LS model predicts only increase in turbulence kinetic energy for all $x/D$. While there is substantial suppression of turbulence, Figure 12 shows that reduction in skin friction coefficient $C_f$ as predicted by the LB, RM, and YS models is only limited to about $x/D \approx 1$. The LS model also predicts a similar magnitude of skin friction reduction as the other three low-Reynolds number turbulence models.

## Conclusions

The phenomenon of turbulence suppression observed experimentally in fully developed pipe flow installed with a ring device at $y^+ = 112$ has been investigated numerically using the standard $k$–$\varepsilon$ model (LS) and three low-Reynolds number $k$–$\varepsilon$ models (LB, RM, and YS). While the LS model (Launder and Spalding 1974) has predicted turbulence suppression in the near-wall region close to the device, it has predicted turbulence enhancement for the main bulk of the flow. On the other hand, all three low-Reynolds number models have predicted turbulence suppression, but the result of the YS model (Yang and Shih 1993) bears

the closest resemblance to the experimental results. However, only a maximum of about 5% turbulence suppression is predicted. The extent of turbulence suppression attributable to a ring device installed at $y^+ = 112$ in developing pipe flow has also been investigated. All three low-Reynolds number models predicted turbulence suppression up to $x/D \approx 30$ with maximum suppression of almost 60% predicted by the YS model. These results indicate that a ring device has a much more significant effect on developing pipe flow than on fully developed flow. On the other hand, the standard LS model predicted only an increase in turbulence kinetic energy for all $x/D$. For both developing and fully developed pipe flows, a ring device installed at $y^+ = 112$ only produces reduction in skin friction for about 1 pipe diameter downstream. On the basis of the numerical results presented here, the standard $k$–$\varepsilon$ model that employs a wall function does not seem to be able to simulate this type of flow. While the results of all three low-Reynolds number models agree qualitatively with each other, they differ in the magnitude of turbulence suppression predicted.

## Acknowledgment

This project was supported by the Australian Research Council. This paper was written while the first author was hosted by Distinguished Professor Max Platzer in the U.S. Naval Postgraduate School with partial support from the National Research Council. The hospitality and support provided by Professor Platzer are gratefully acknowledged.

## References

Coustols, E. and Savill, A. M. 1992. Turbulence skin friction drag reduction by active and passive means: Part 2. AGARD Rep. 786, 8:55–80

Chien, K. Y. 1982. Predictions of channel and boundary-layer flows with a low-Reynolds number turbulence model. *AIAA J.* **20**, 33–38

Hollis, P. G. Lai, J. C. S. and Bullock, K. J. 1992. What happens if a LEBU device is inserted in the near-wall region? *Proc. 11th Australasian Fluid Mech Conference*, Hobart, Tasmania, Australia, 547–550.

Khoo, B. C., Chew, Y. T. and Mah, Y. A. 1993. Skin friction following BLADE manipulation in a turbulent pipe flow. *Exper. Fluids*, **15**, 274–278

Kim, J., Moin, P. and Choi, H. 1990. Active turbulence control in a wall-bounded flow using direct numerical simulations. In *Structure of Turbulence and Drag Reduction*, A. Gyr (ed.) (IUTAM Symposium Zurich, Switzerland, July 25–28), Springer-Verlag, Berlin

Laufer, J. 1954. The structure of turbulence in fully developed pipe flow. NACA 1174

Lam, C. K. G. and Bremhorst, K. 1981. A modified form of the $k$–$\varepsilon$ model for predicting wall turbulence. *J. Fluids Eng.*, **103**, 456–460

Launder, B. E. and Sharma, B. I. 1974. Application of the energy-dissipation model of turbulence to calculation of flow near a spinning disc. *Lett. Heat Mass Transfer*, **1**, 131–138

Launder, B. E. and Spalding, D. B. 1974. The numerical computation of turbulent flows. *Comp. Meth. Appl. Mech. Eng.* **3**, 269–298

Mah, Y. A. Khoo, B. C. and Chew, Y. T. 1992. The effect of BLADE manipulator in fully developed pipe flow. *J. Fluids Eng.*, **114** 687–689

Nikuradse, J. 1933. Stromungsgesetze in rauhen Rohren. forschg. Arb. Ing.—Wes. No. 361 (quoted in *Boundary Layer Theory*, H. Schlichting, 7th ed. McGraw Hill, New York, 618)

Patankar, S. V. 1980. *Numerical Heat Transfer and Fluid Flow*. Hemisphere, Bristol, PA, 1090–1093

Patel, V. C., Rodi, W. and Scheuerer, G. 1985. Evaluation of turbulence models for near-wall and low-Reynolds number flows. *AIAA J.*, **23** 1308–1319

Pollard, A., Savill, A. M. and Thomann, H. 1989. Turbulent pipe flow manipulation: Some experimental and computational results for single manipulator rings. *Appl. Sci. Res.*, **46**, 281–290

Pollard, A., Thomann, H. and Savill, A. M. 1990. Manipulation and modelling of turbulent pipe flow: Some parametric studies of single and tandem ring devices. *Proc. 4th European Drag Reduction Meeting*, E. Coustols (ed.) (Lausanne, Switzerland, July 24 1989), Kluwer Academic Publishers, the Netherlands, 23–40

Pun, W. M. and Spalding, D. B. 1976. A General computer program for two-dimensional elliptic flows. HTS/76/2, Imperial College

Prabhu, A., Vasudevan, B., Kailasnath, P., Kulkarni, R. S. and Narasimha, R. 1987. Blade manipulators in channel flow. *Proc. Turbulence Management and Relaminarisation IUTAM Symposium*, H. W. Liepmann and R. Narasimha (eds.) (Bangalore, India), 97–106

Richman, J. W. and Azad R. S. 1973. Developing turbulent flow in a smooth pipe. *Appl. Sci. Res.*, **28** 419–441

Rodi, W. and Mansour, N. N. 1993. Low-Reynolds number $k$–$\varepsilon$ modeling with the aid of direct simulation data. *J. Fluid Mech.*, **250**, 509–529

Sahlin, A., Johansson, A. V. and Alfredsson, P. H. 1988. The possibility of drag reduction by outer layer manipulators in turbulent boundary layers. *Phys. Fluids*, **31**, 2814–2820

Savill A. M. and Mumford, J. C. 1988. Manipulation of turbulent boundary layers by outer-layer devices: Skin-friction and flow-visualization results. *J. Fluid Mech.*, **191**, 389–418

Savill A. M., Klein, H. and Friedrich, R. 1993. Pattern recognition analysis of structure in manipulated channel flow simulations. In *Eddy Structure Identification in Free Turbulent Flows*, J. P. Buritzel and M. N. Clauser (eds.) Kluwer Academic Publishers, The Netherlands, 195–211

Squire, L. C. and Savill, A. M. 1996. Experimental results on aerofoil manipulators at high subsonic speeds. *Exper. Fluids*, **21**, 275–285

Wark, C. E., Naguib, A. M. and Nagib, H. M. 1990. Effect of plate manipulators on coherent structures in a turbulent boundary layer. *AIAA J*, **28**, 1877–1884

Wilcox, D. C. and Rubesin, W. M. 1980. Progress in turbulence modeling for complex flow fields including effects of compressibility. NASA 1517

Yang, Z. and Shih, T. H. 1993. New time-scale-based $k$–$\varepsilon$ model for near-wall turbulence. *AIAA J.*, **31**, 1191–1198

Yang, C. and Lai, J. C. S. 1993. The calculation of incompressible turbulent developing pipe flow. The University of New South Wales, University College, Research Rep., June, 1993, NSW, Australia